

1 **Enhanced climate response to ozone depletion from**
2 **ozone-circulation coupling**

3 **Pu Lin^{1,2}, and Yi Ming²**

4 ¹Program in Atmospheric and Oceanic Sciences, Princeton University, Princeton, NJ

5 ²NOAA/Geophysical Fluid Dynamics Laboratory

6 **Key Points:**

- 7 • Interactive ozone schemes produce stronger stratospheric cooling than prescrib-
8 ing the same ozone changes.
- 9 • Dynamical response to ozone depletion drives the difference in temperature response.
- 10 • A cheap interactive ozone scheme is developed and behaves similarly to the full
11 chemistry scheme.

Corresponding author: Pu Lin, pulin@princeton.edu

Abstract

The effect of stratospheric ozone depletion is simulated in GFDL AM4 model with three ozone schemes: prescribing monthly zonal mean ozone concentration, full interactive stratospheric chemistry, and a simplified linear ozone chemistry scheme but with full dynamical interactions. While similar amounts of ozone loss are simulated by the three schemes, the two interactive ozone schemes produce significantly stronger stratospheric cooling than the prescribed one. We find that this temperature difference is driven by the dynamical responses to ozone depletion. In particular, the existence of ozone hole leads to strong ozone eddies that are in-phase with the temperature eddies. The coherence between ozone and temperature anomalies leads to a weaker radiative damping as ozone absorbs shortwave radiation that compensates for the longwave cooling. As a result, less wave dissipates at the lower stratosphere, leading to a weaker descending and dynamical heating over the polar lower stratosphere, and hence a stronger net cooling there. The covariance between ozone and temperature is largely suppressed when ozone is prescribed as monthly zonal mean time series, as is the reduction in the radiative damping following ozone depletion. With much lower computational cost, the simplified ozone scheme is capable of producing similar magnitude of ozone loss and the consequent dynamical responses to those simulated by the full chemistry.

Plain Language Summary

It is well-known that the ozone hole over Antarctica leads to a strong cooling in the stratosphere. However, when simulating this effect in climate models, we find that the magnitude of the cooling depends on how ozone is represented in the model. Compared to the model specifying ozone concentrations as monthly time series, stronger cooling is found in the model calculating ozone concentrations from the photochemical reactions. This is because the spatial distribution and the short-term temporal variation of ozone are not consistent with the circulation when ozone is specified, which leads to a stronger over-turning circulation with ascending branch over the tropics and descending branch over the polar region. The stronger descending motion then drives a stronger dynamical heating that compensates for the radiative cooling induced by ozone loss. As a result, a weaker net cooling is produced in the model with specified ozone. We also test a model in which ozone is allowed to vary with the circulation, but the chemical processes are greatly simplified. The computational cost of this model is much cheaper than the

44 one that incorporates the photochemical reactions, but the magnitude of the simulated
45 stratospheric cooling is similar.

46 **1 Introduction**

47 Stratospheric ozone changes impose a significant forcing to the climate system. The
48 depletion of stratospheric ozone occurring over the past few decades has been credited
49 with being a major driver for circulation changes, especially over the Southern Hemi-
50 sphere (Solomon, 1999; Polvani et al., 2011). Despite its importance, most climate mod-
51 els do not simulate the chemical reactions producing and depleting ozone, but prescribe
52 monthly time series of ozone concentration instead (Eyring et al., 2013; Gerber & Son,
53 2014; Checa-Garcia et al., 2018; Keeble et al., 2020). Computational cost is a major hur-
54 dle for climate models to include full stratosphere chemistry.

55 While the radiative cooling in the stratosphere is certainly the leading effect of ozone
56 depletion, it has long been suspected that there may be non-trivial chemical and dynam-
57 ical feedbacks to ozone changes that are not represented by prescribing monthly ozone
58 time series. This motivates comparisons between the models participating the Coupled
59 Model Intercomparison Project (CMIP) phase 3 and 5 and the chemistry climate mod-
60 els which incorporate fully interactive ozone. The multi-model means of the two groups
61 do not always show a clear distinction in terms of responses to ozone depletion (Son et
62 al., 2008, 2010; Gerber & Son, 2014), which may not be surprising given the large struc-
63 tural difference among models. A more appropriate comparison would be utilizing a sin-
64 gular model where the only change between simulations is how ozone is represented. Such
65 single model studies show that the interactive ozone leads to stronger response to ozone
66 depletion in the Southern Hemisphere (Gillett et al., 2009; Waugh et al., 2009; Neely et
67 al., 2014; Li et al., 2016; Haase et al., 2020), and stronger variability in the Northern Hemi-
68 sphere polar region (Haase & Matthes, 2019; Rieder et al., 2019).

69 It is important to recognize that prescribing ozone not only ignores the interaction
70 between the chemical reactions and the background meteorological conditions, but also
71 suppresses the coupling between ozone and circulation. Earlier studies have attributed
72 the difference between the simulations with and without full chemistry to the zonal asym-
73 metry in the ozone concentration (Gillett et al., 2009; Waugh et al., 2009). This moti-
74 vated CMIP6 models to specify longitudinally-varying ozone instead of zonal mean (Checa-

75 Garcia et al., 2018; Keeble et al., 2020). Rae et al. (2019) further proposed a scheme to
76 redistribute ozone according to the potential vorticity (PV) field. This inexpensive mod-
77 ification brings about an ozone field that is more consistent with the dynamics, and is
78 found to greatly ease the bias in the Northern Hemisphere, but is not helpful and even
79 causes stronger bias in the Southern Hemisphere (Rae et al., 2019). A recent study by
80 Neely et al. (2014) showed that specifying monthly mean ozone concentrations effectively
81 dampens the temporal variation, leading to significantly weaker ozone loss realized by
82 the model. They hence proposed to prescribe daily zonal mean ozone instead of monthly
83 mean.

84 In this study, we revisit the issue of how ozone depletion affects the climate sys-
85 tem using the GFDL AM4 model (Zhao et al., 2018a, 2018b). We compare the simula-
86 tions of AM4 with full stratospheric chemistry against the ones with specified monthly
87 zonal mean ozone concentrations. In addition, we introduce a new scheme to represent
88 ozone variations in the model, which is computationally as cheap as specifying ozone.
89 We find that specifying monthly zonal mean ozone underestimates the effect of ozone
90 depletion, but the new scheme can reproduce the magnitude of the springtime strato-
91 spheric cooling simulated in the full chemistry simulations. The physical process lead-
92 ing to the biases in prescribing monthly zonal mean ozone is identified and assessed. In
93 the following, we will first give a detailed description of the simulations in section 2, then
94 the results are presented in section 3, which is followed by a summary and discussion in
95 section 4.

96 **2 Model and Experiments**

97 In this study, we employ the GFDL AM4 (Zhao et al., 2018a, 2018b), the atmo-
98 spheric component of the GFDL’s coupled physical model CM4 (Held et al., 2019). We
99 follow the model configuration documented by Zhao et al. (2018b) except that the model
100 top is raised from 1 hPa to 0.01 hPa, and the vertical resolution is increased from 33 lev-
101 els to 63 levels. This is to ensure sufficient resolution to resolve the stratosphere. De-
102 spite the difference in the model top and the vertical coordinate, the simulated tropo-
103 sphere and surface climate are generally similar to those reported by Zhao et al. (2018a).

104 The default AM4 consists of a light tropospheric chemistry scheme and prescribes
105 monthly zonal mean ozone concentration. Simulations with this setting are referred to

106 as control (CNTL) in this study. We also perform simulations with fully interactive chem-
 107 istry (FullChem) using the chemistry scheme as in the GFDL earth system model ESM4
 108 (Dunne et al., 2020) and AM4.1 (Horowitz et al., 2020). The stratospheric chemistry for-
 109 mulation and its performance is documented by Austin and Wilson (2006).

110 In addition, we design a simplified ozone scheme, in which ozone is treated as a
 111 tracer in the model that can be freely transported by circulation as in FullChem, but the
 112 chemical tendency of the tracer is reduced to the following:

$$\frac{D[O3]}{Dt} \Big|_{chem} = P - \frac{[O3]}{\tau} \quad (1)$$

113 where $[O3]$ is the ozone concentration, P is the chemical production rate of ozone, and
 114 τ is the chemical lifetime. Derivation and samples of P and τ are given in the Appendix.
 115 Both P and τ are specified in the model as monthly zonal mean time series. This scheme
 116 thus allows full dynamical interaction between ozone and circulation while restraining
 117 the chemical interactions. Simulations with this ozone scheme are referred to as O3Tracer.

118 There have been several simplified stratospheric ozone schemes that specify the chem-
 119 ical tendency as a linear function of ozone concentration, temperature and partial col-
 120 umn of ozone, with additional terms to account for the heterogeneous reactions (e.g., Car-
 121 iolle & Déqué, 1986; McLinden et al., 2000; McCormack et al., 2004). These linear schemes
 122 are widely used in the numerical weather models that have more stringent constraints
 123 on computational cost. The application of the linear ozone scheme to the climate mod-
 124 els are much rarer, with noticeable exceptions of the climate models from CNRM (Voltaire
 125 et al., 2013; Michou et al., 2019) and the recent E3SM (Golaz et al., 2019). The coef-
 126 ficients are usually derived from an off-line chemistry model specified with a certain me-
 127 teorological state, and often lead to spurious results for the severe ozone depletion over
 128 the Antarctica that are highly nonlinear (Geer et al., 2007; Monge-Sanz et al., 2011; Eyring
 129 et al., 2013). To some extent, our O3Tracer scheme is a simplified version of these lin-
 130 ear ozone schemes. However, by prescribing different P and τ for different climate states,
 131 all the chemical changes are factored in regardless whether they are linear or nonlinear
 132 with respect to the meteorological states. As will be shown below, the two terms in Eq.
 133 1 are sufficient to capture the bulk of ozone loss.

134 We conduct a pair of time-slice experiments with each ozone schemes: *1960O3* and
 135 *2010O3*. For FullChem, ozone depleting substances are set to either year 1960 or 2010
 136 level, corresponding to the unperturbed and depleted states, respectively. The CNTL

137 and O3Tracer simulations then take the monthly zonal mean climatology from the cor-
 138 responding FullChem simulations. All other forcings and SST/SICs are set to year 2010
 139 level, and are identical in all simulations. Each simulation is run for 80 years, and the
 140 first 10 years are considered as the spin-up and discarded. Most analyses are focused in
 141 the lower stratosphere over the Southern Hemisphere polar region, where the ozone de-
 142 pletion is the severest.

143 In addition, we use the Fu-Liou radiative transfer model (Fu & Liou, 1992; Rose
 144 & Charlock, 2002) to calculate the radiative effect of ozone changes. The off-line radia-
 145 tive transfer calculation assumes clean-sky condition (i.e., no clouds or aerosols), and uses
 146 November mean zonal mean profiles of temperature, ozone, and water vapor concentra-
 147 tion, and surface albedo from the corresponding simulations. The calculation uses the
 148 four-stream algorithm, and a one-day calculation is done for 16 November. Note that
 149 this is not the radiative transfer model used in AM4, but the difference due to radiative
 150 schemes is generally small. In general, Fu-Liou radiative transfer model is more expen-
 151 sive and more accurate than those used in GCMs.

152 **3 Results**

153 We start by comparing the ozone loss and the stratospheric cooling simulated by
 154 the three ozone schemes. Figure 1 a and b show the ozone and temperature difference
 155 at 100 hPa over the southern polar cap between the *2010O3* and *1960O3* simulations.
 156 Reduction of ozone is seen throughout the year with the strongest depletion in October.
 157 Consequently, cooling is found over the lower stratospheric polar region, which peaks in
 158 November. However, the magnitudes of the cooling among the three simulations are not
 159 proportional to their ozone loss. O3Tracer produces weaker ozone loss than the other
 160 two. Yet, its resulting cooling is as strong as that in FullChem. It is CNTL that yields
 161 the weakest cooling, despite its almost identical ozone loss to FullChem. In November,
 162 O3Tracer produces $1.8K$ or 26% more cooling than CNTL, and the difference between
 163 Fullchem and CNTL is $2.3K$ or 32%. The difference in the stratospheric cooling between
 164 CNTL and the other two are statistically significant at the 95% confidence level.

165 To interpret this difference in temperature responses, we analyze the heat budget.
 166 In the stratosphere, the leading components of the heat budget are the longwave and short-
 167 wave radiation as well as dynamical heating, which is brought about by advection of var-

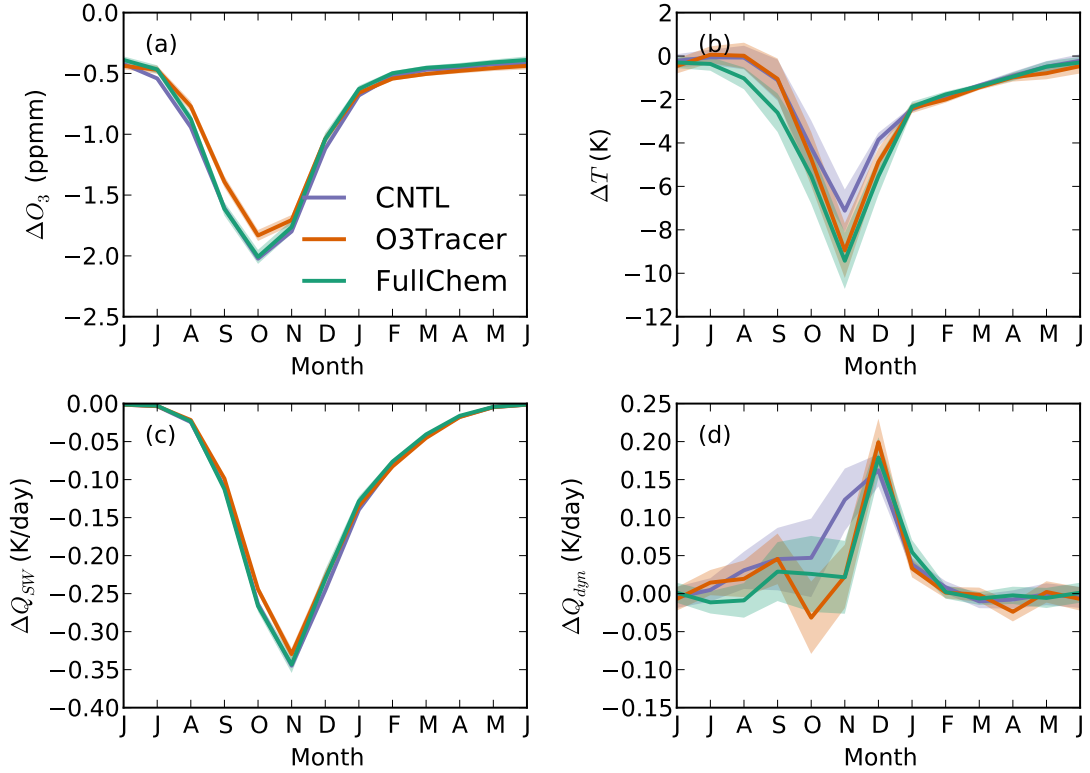


Figure 1. Difference in (a) ozone concentration, (b) temperature, (c) shortwave (SW) heating rate, and (d) dynamical heating rate between the *2010O3* and the *1960O3* experiments. Purple lines are for the CNTL simulation, orange lines are for the O3Tracer simulation, and green lines are for the FullChem simulation. Results are shown at 100 hPa averaged over 60°S and 90°S. Shading indicates the 95% uncertainty range estimated based on the Student's t-test.

168 ous scales. Following ozone depletion, temperature changes are driven by a reduction
169 of shortwave heating as well as changes in the dynamical heating, whereas longwave ra-
170 diation largely responds to the temperature variations. As shown in Fig. 1c, similar amounts
171 of decrease in shortwave heating rate are seen among the three simulations. On the other
172 hand, CNTL simulates more dynamical heating than the other two experiments in re-
173 sponse to ozone loss (Fig. 1d). The difference in dynamical heating response is most sig-
174 nificant in November, when CNTL yields 0.12 K per day more dynamical heating, whereas
175 O3Tracer and FullChem show no significant change. Comparing changes in the radia-
176 tive and dynamical heating rates, it is clear that the dynamical heating rates drive the
177 diversified temperature responses to ozone depletion in these simulations. Similar results
178 are found at other levels in the lower stratosphere and are not shown.

179 Focusing on November when the difference in dynamical heating rate and temper-
180 ature is the largest between CNTL and O3Tracer or FullChem, we investigate the cause
181 of the dynamical heating over the polar stratosphere. The stratosphere is dominated by
182 the Brewer-Dobson circulation (Butchart, 2014, and references therein), an overturning
183 circulation ascending over the low-latitudes and descending over the high-latitudes. An
184 adiabatic warming then results from the descending over the polar region. The strength
185 of the circulation is described by the Transformed Eulerian mean (TEM) velocities, and
186 the dynamical heating rate over the stratospheric polar region is proportional to the TEM
187 vertical velocity w^* . Figure 2a plots the TEM vertical velocity w^* averaged over the po-
188 lar region from the three *201003* simulations. While all three simulations show descend-
189 ing throughout the stratosphere, the descending in CNTL is stronger than O3Tracer or
190 FullChem in the lower stratosphere, and weaker above.

191 Because the Brewer-Dobson circulation is a wave-driven circulation, its strength
192 is tightly linked to wave dissipation in the stratosphere. As shown in Fig. 2b, waves typ-
193 ically propagate upward from the troposphere into the stratosphere over mid-latitudes,
194 and dissipate over a broad region over the stratospheric extratropics. Compared to CNTL,
195 both O3Tracer and FullChem show less wave dissipation over the lower half of the strato-
196 sphere, and more wave dissipation above (Fig. 2c and 2d). This is consistent with the
197 w^* shown in Fig. 2a as downward control principle indicates that w^* at a certain level
198 should be proportional to the integrated wave dissipation above that level (Haynes et
199 al., 1991).

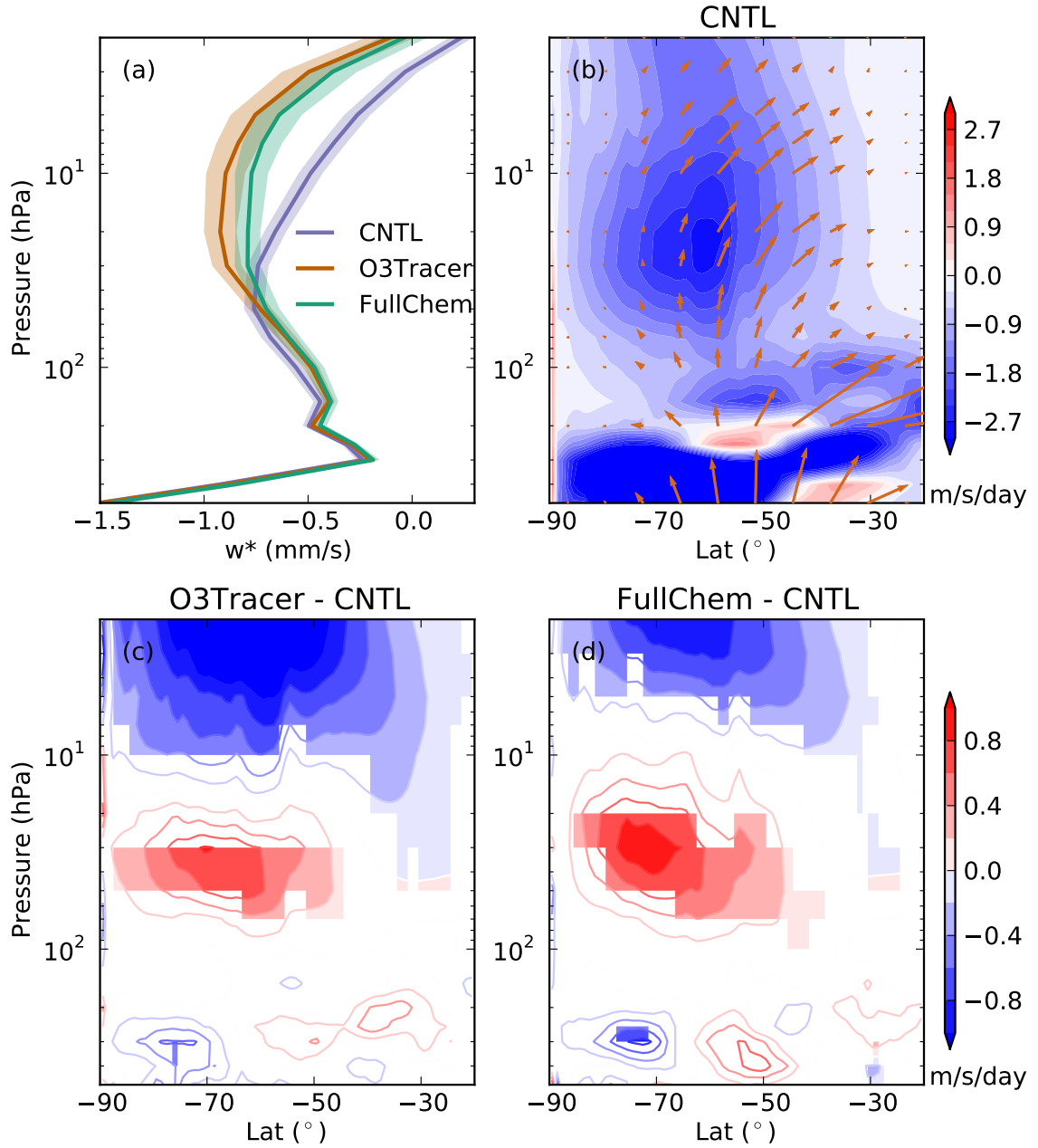


Figure 2. Dynamical conditions in November from the *201003* experiment. (a) TEM vertical velocity w^* averaged over 60°S - 90°S . Shading indicates the 95% uncertainty range estimated based on the Student's *t*-test. (b) EP flux (vectors) and its divergence (shadings) simulated in the CNTL simulation. (c) Difference in EP flux divergence between the O3Tracer and the CNTL simulations. Contours are filled where the difference is statistically significant at 95% confidence level based on the Student's *t*-test. (d) As in (c), except for the FullChem simulation. Note that a more negative EP flux divergence indicates more wave dissipation, and vice versa.

200 A key factor controlling wave propagation and dissipation is the background zonal
 201 winds. Linear theory predicts that the upward wave propagation is suppressed when the
 202 stratospheric jet is easterly or strong westerly, and strong dissipation occurs when the
 203 background zonal wind matches with the phase speed (Charney & Drazin, 1961). There-
 204 fore, stronger Brewer-Dobson circulation and stronger dynamical heating over the po-
 205 lar region are expected when the stratospheric jet is moderately westerly. This relation-
 206 ship is confirmed in Fig. 3 which plots the seasonal cycle of the dynamical heating rate
 207 and the strength of polar night jet. The *2010O3* experiments show a delayed seasonal
 208 cycle in both dynamical heating rates and zonal wind compared to the *1960O3* exper-
 209 iments. But when plotting the dynamical heating rate against the zonal wind, the two
 210 experiments share similar characteristics: dynamical heating rate peaks around zonal wind
 211 of 20 m/s and diminishes quickly when zonal wind approaches zero as well as increases
 212 towards higher values. A secondary peak of dynamical heating rate locates around 10
 213 m/s in austral autumn. The response of dynamical heating to ozone depletion is then
 214 explained by zonal winds. Ozone depletion strongly cools the polar stratosphere, which
 215 leads to a stronger polar night jet following the thermal wind balance. During late spring/early
 216 summer, the wave-wind relationship is in the weak westerly regime, so that a small in-
 217 crease in zonal winds leads to extensive strengthening of the circulation and dynamical
 218 warming over the polar region.

219 However, the difference between CNTL and O3Tracer or FullChem cannot be ex-
 220 plained by zonal winds. As shown in Fig. 3c, the *2010O3* simulation with O3Tracer or
 221 FullChem shows a weaker dynamical heating than others under the same zonal wind con-
 222 ditions. The disparity is most perceivable when zonal wind is between 20 to 30 m/s, which
 223 coincides with November in the *2010O3* simulations. We argue that the responsible pro-
 224 cess for this difference in the dynamical heating rate and wave dissipation is the radia-
 225 tive damping of the waves.

226 Radiative damping comes from the basic principle of radiation that a warmer air
 227 parcel emits more longwave radiation and hence cools faster, which acts to diminish ther-
 228 mal anomalies. The dissipation from the radiative damping is usually considered as a
 229 small term compared to the dissipation induced by zonal winds. However, the zonal wind-
 230 induced dissipation is confined to waves of certain phase speed that match with the back-
 231 ground zonal winds. The radiative damping, on the other hand, does not have such re-
 232 striction, and the cumulative effect may not be trivial. Such difference allows us to dis-

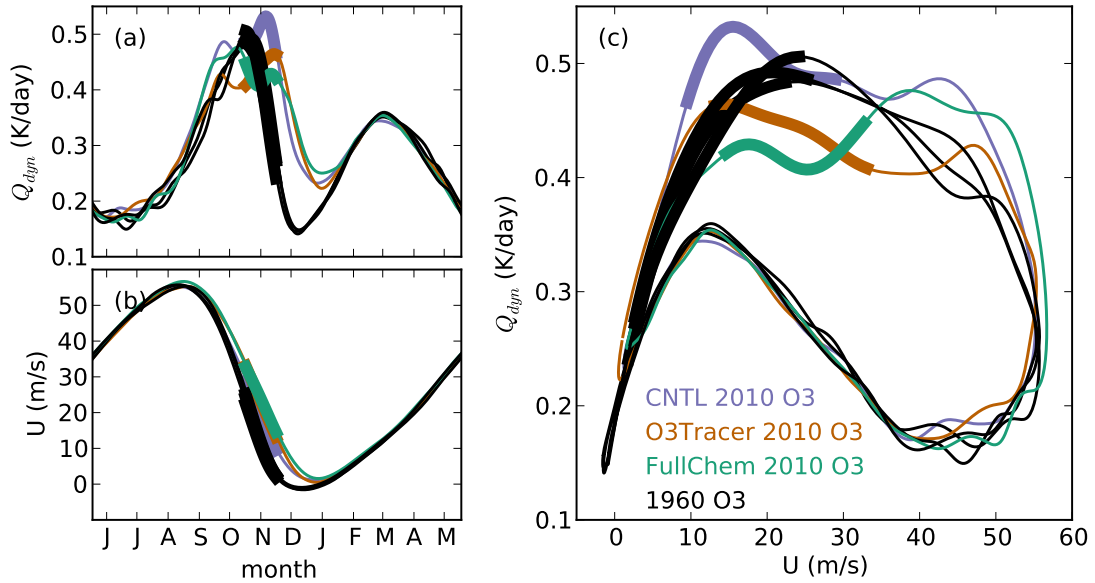


Figure 3. Seasonal cycle of (a) dynamical heating rate at 100 hPa averaged over 60°S–90°S, and (b) zonal mean zonal wind at 50 hPa 60°S. (c) The two seasonal cycle plotted against each other. Seasonal cycles are calculated using daily mean data averaged over the last 70 years of the simulation and then smoothed by a Gaussian kernel with standard deviation of 7 days. November days are marked by the thicker lines. Purple lines are for the CNTL *2010O3* simulations, orange lines are for the O3Tracer *2010O3* simulations, green lines are for the FullChem *2010O3* simulations, and black lines are for the *1960O3* simulations.

233 distinguish the two types of wave dissipation in the phase speed spectra. Figure 4 shows
 234 the difference in wave dissipation between the *2000O3* and the *1960O3* experiments as
 235 a function of angular phase speed and latitude in November at 50 Pa. In the CNTL case,
 236 less dissipation (positive anomalies) occurs at the lower phase speed, and more dissipa-
 237 tion (negative anomalies) occurs at the higher phase speed over high latitudes. Such a
 238 shift of wave dissipation towards higher phase speed is consistent with the strengthen-
 239 ing of the polar night jet following ozone depletion. This again confirms that the dynam-
 240 ical response to ozone depletion in the CNTL experiment largely comes from the zonal
 241 wind-induced wave dissipation.

242 The changes of wave dissipation simulated from O3Tracer and FullChem (Fig. 4b
 243 and 4c) show a more complex pattern than that from CNTL (Fig. 4a). This is because
 244 more than one process is at work. We decompose the wave dissipation changes from O3Tracer
 245 and FullChem into two components. The first is constructed by subtracting the CNTL
 246 *2010O3* wave dissipation spectra from the corresponding O3Tracer and FullChem ones,
 247 shown in Figs. 4d and 4e. The second component is simply the residual, shown in Figs.
 248 4f and 4g. We find the second components of O3Tracer and FullChem bear strong simi-
 249 larity to the wave dissipation changes of CNTL, showing wave dissipation shifts towards
 250 higher phase speed over high latitudes. The first component, on the other hand, shows
 251 an omnipresent reduction of the wave dissipation with a pattern similar to its climatol-
 252 ogy. We argue that the first component reflects changes in the radiative damping, while
 253 the second component is related to the changes in zonal winds.

254 It is then natural to ask why ozone depletion leads to a weakening of radiative damp-
 255 ing in simulations of interactive ozone but not in ones with ozone prescribed. We pro-
 256 pose that the weakening of radiative damping comes from the coherence between tem-
 257 perature and ozone anomalies so that warmer air parcel consists of higher ozone concen-
 258 tration. This anomalous ozone absorbs shortwave radiation that partly cancels the long-
 259 wave cooling, yielding weaker radiative damping.

260 The coherence between temperature and ozone has been observed as early as the
 261 beginning of the satellite era (Newman & Randel, 1988). This is because the long life-
 262 time of ozone in the lower stratosphere makes it a quasi-conservative tracer following the
 263 motion of air parcels. Potential temperature and potential vorticity (PV) are also quasi-
 264 conservative tracers for motions on timescales of less than a few weeks (Andrews et al.,

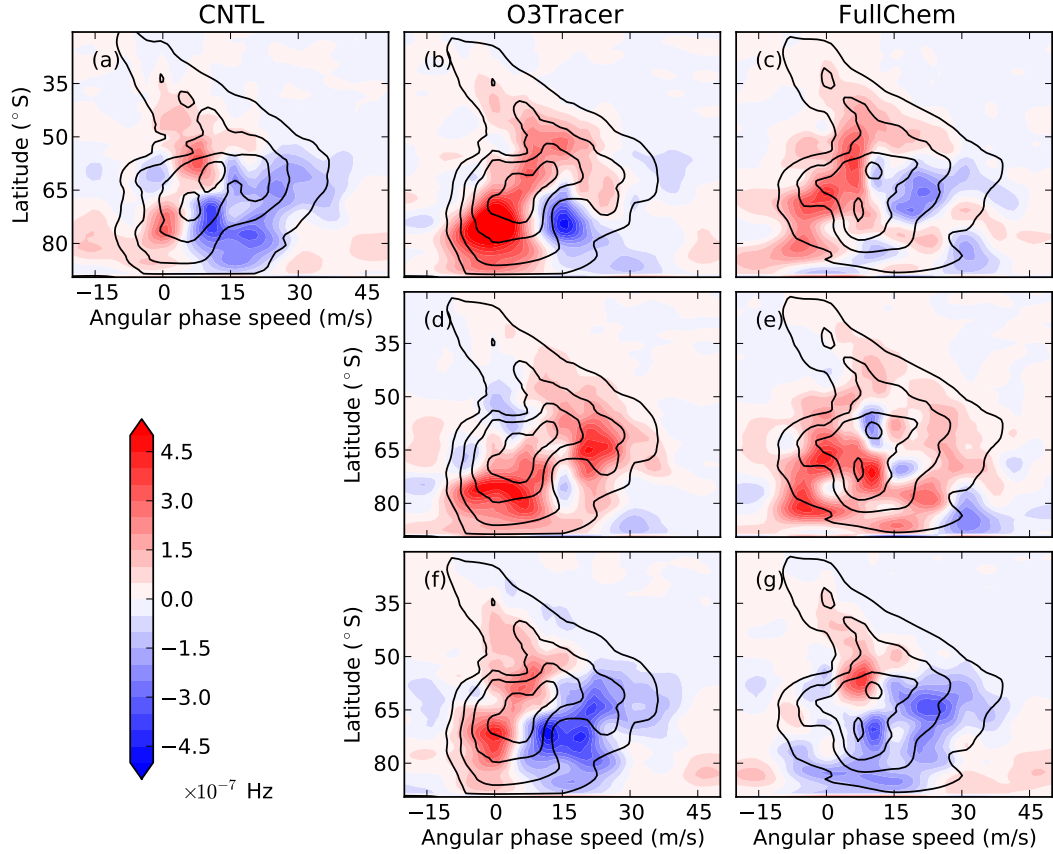


Figure 4. Difference in the phase speed spectra of EP flux divergence at 50 hPa in November between the *2010O3* and the *1960O3* experiments from (a) CNTL, (b) O3Tracer and (c) FullChem simulations. (d) The first component of the spectral responses to ozone depletion simulated in O3Tracer, calculated by subtracting the CNTL *2010O3* from the O3Tracer *2010O3*. (f) The second component of the spectral response to ozone depletion in O3Tracer, calculated as the residual of the first component. (e) and (g) as in (d) and (f), except for the FullChem simulation. Black contours plot the climatology from the *1960O3* experiment at $-9, -7, \dots, -1 \times 10^{-7}$ Hz.

265 1987). Therefore, ozone, temperature and PV are expected to co-vary with each others
266 in the lower stratosphere. As shown in Fig. 5, strong PV gradient is found surrounding
267 the pole, which acts as a barrier between the cold and low-ozone air over the pole and
268 the warm and high-ozone air on the equator side (Schoeberl & Hartmann, 1991). These
269 PV contours never lie perfectly parallel with the latitudinal lines. Instead, they are un-
270 dergoing constant deformation and displacement while redistributing the air, and hence
271 creating eddies of temperature and ozone along latitudes. Both temperature and ozone
272 anomalies are therefore closely tied to the PV anomalies.

273 The magnitudes of the ozone and temperature eddies depend on the contrast across
274 the PV gradient barrier. During the ozone depletion era, catalytic reactions occurring
275 on the surface of the polar stratospheric clouds strongly deplete ozone inside the polar
276 vortex (Fig. 5b). During the pre-depletion era, on the other hand, the ozone concentra-
277 tion does not differ much inside and outside the vortex (Fig. 5d). This is not only due
278 to the absence of the catalytic reactions, but also due to the weak vortex in November
279 during the pre-depletion era that are susceptible for air outside the vortex to mix in. There-
280 fore, the same PV perturbation would yield much weaker ozone anomalies in the pre-
281 depletion era. This explains why there is no distinguishable difference in the *1960O3* ex-
282 periments whether ozone is allowed to interact with circulation or not (black lines in Fig.
283 3).

284 The extent of this ozone-circulation interaction depends on the extent of the ozone
285 hole. We therefore expect this interaction has weak effect over low latitudes. The ozone
286 hole is largely confined within the altitudes between 12 and 24 km (Solomon et al., 2005),
287 which is roughly consistent with the weakening of wave dissipation (positive anomalies)
288 shown in Fig. 2c and 2d. The stronger wave dissipation (negative anomalies) seen at the
289 higher levels in Figs. 2c and 2d, on the other hand, is not directly due to the ozone-circulation
290 interaction. Rather, it results from the fact that more waves can reach the upper strato-
291 sphere since they are less attenuated at the lower levels. The stronger wave dissipation
292 at the upper stratosphere extends into the low latitudes as the waves turn equator-ward
293 at this altitude (Fig. 2b).

294 The timing of the ozone-circulation interaction is affected by several factors. Po-
295 lar vortex needs to be strong enough to hold a severe ozone hole, but also not too strong
296 so that waves can enter the stratosphere and disturb the vortex. At the same time, stronger

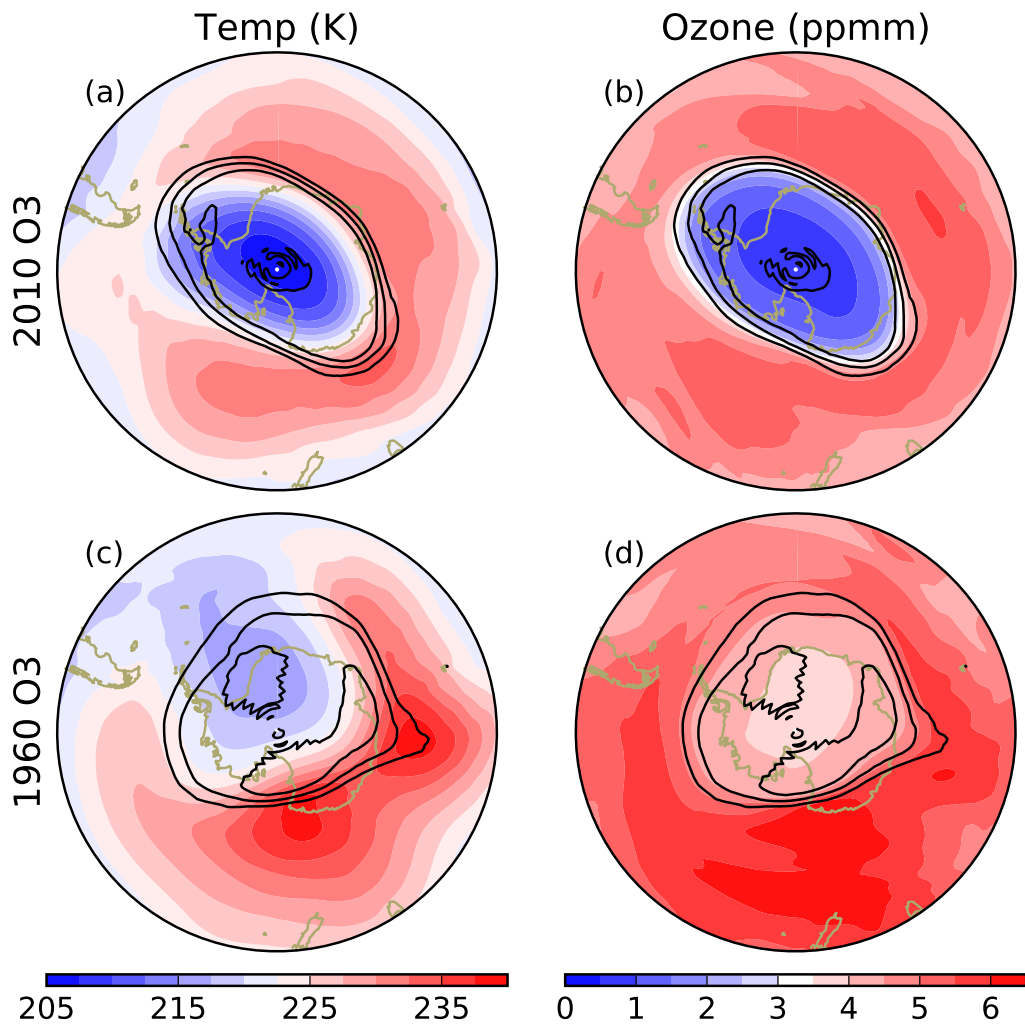


Figure 5. Snapshot of (a) temperature and (b) ozone concentration at 50 hPa from a random day in November from the *2010O3* O3Tracer simulation. (c) and (d) as in (a) and (b), except from the *1960O3* simulation. Black contours plot PV at -50, -60, and -70 PVU.

297 insolation is a favorable condition as the ozone-circulation interaction originates from
298 the absorption of solar radiation by ozone. November is the optimal time for the ozone-
299 circulation interaction to take effect given these conditions.

300 To quantify the effect of the ozone-circulation interaction on the radiative damp-
301 ing, we calculate the effective radiative damping rate following Hitchcock et al. (2010).
302 We regress the daily radiative heating rate anomalies against temperature anomalies with
303 zonal mean and climatological seasonal cycle removed. The resulting slope is the effec-
304 tive radiative damping rate, and the reciprocal of the slope is the radiative damping time
305 scale. Figure 6 shows the regression from the three *2010O3* simulations at 60°S 50 hPa
306 as an example. The three simulations show a similar damping rate of 0.06 day^{-1} for long-
307 wave radiation. When shortwave radiation is included, the damping rate in CNTL is not
308 affected, but both O3Tracer and FullChem show a reduction of the radiative damping
309 rate. This reduction comes from the shortwave absorption by the ozone anomalies that
310 accompany the temperature anomalies. Figure 6d and 6e further show the distributions
311 of the shortwave contribution to the radiative damping in O3Tracer and FullChem, which
312 are generally consistent with the wave dissipation anomalies shown in Fig. 2c and 2d.
313 Shortwave radiation leads to a reduction of the radiative damping throughout the lower
314 stratosphere. The strongest reduction exceeding 50% is found near 50 hPa over high lat-
315 itudes.

316 Lastly, we use an offline radiative transfer model to quantify the effect of the ozone-
317 circulation interaction. We regress ozone anomalies upon temperature anomalies as we
318 did with heating rates. The resulting ozone anomaly associated with 1K warming is added
319 to the climatological mean profiles. We use Fu-Liou radiative transfer model (Fu & Liou,
320 1992; Rose & Charlock, 2002) to calculate the shortwave heating rate changes due to the
321 ozone changes. The resulting heating rate changes are compared to the effective radia-
322 tive damping rates from the aforementioned regression analysis. Figure 7 shows the com-
323 parison at 50 hPa. Agreement is found between the off-line radiative transfer calcula-
324 tion and the regression analysis. Similar agreement is also found at other levels but not
325 shown here. The agreement between the two methods confirms that the shortwave's con-
326 tribution to the radiative damping arises from the ozone anomalies associated with the
327 temperature anomalies.

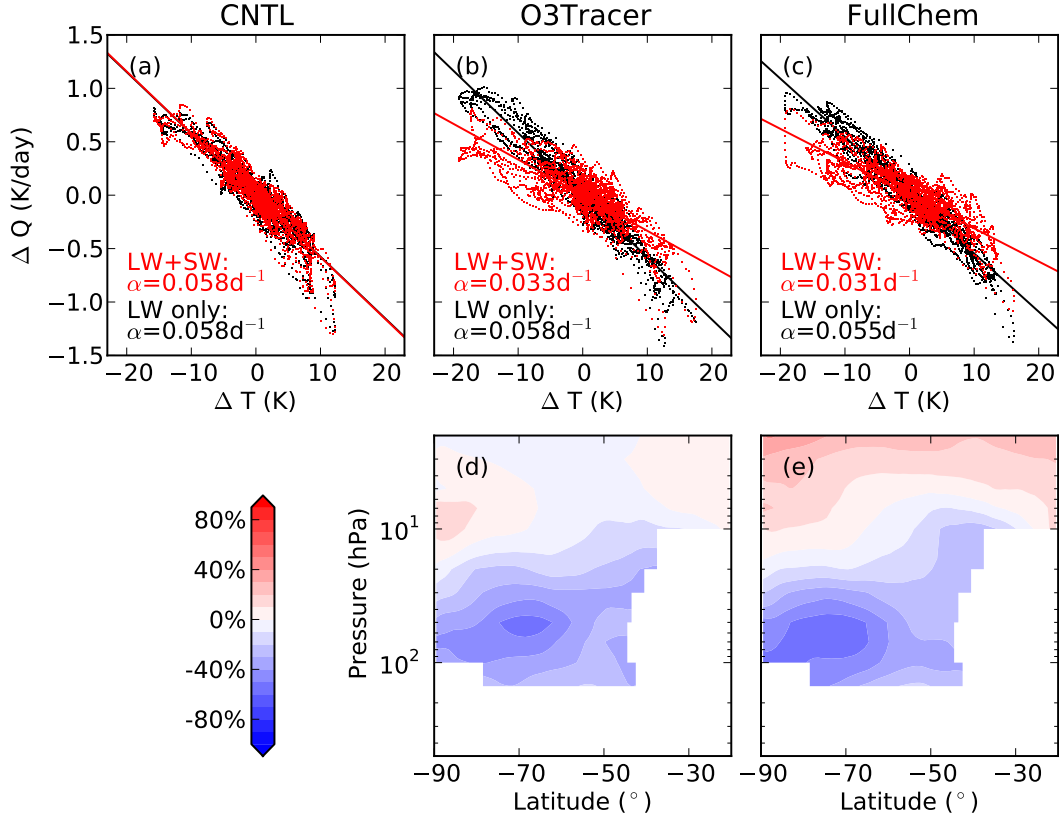


Figure 6. Scatter plot of radiative heating rate anomalies versus temperature anomalies on 15 November at 50 hPa 60°S in *2010O3* experiment from (a) CNTL, (b) O3Tracer, and (c) FullChem simulations, and relative contribution to the effective radiative damping rates from the shortwave radiation from (d) O3Tracer and (e) FullChem simulations. The anomalies are calculated by subtracting the zonal mean and the 10 year mean of the same date. For clarity, only 10 years of data are shown. Results are similar using the full length of the simulation. Black dots show the longwave (LW) radiative heating rates, and red dots show the combined heating rates from both longwave and shortwave (SW) radiation. The effective damping rate calculated from the linear orthogonal regression is listed in the legend. Relative contribution to the effective radiative damping rates from the shortwave radiation is calculated as $(\alpha_{LW+SW} - \alpha_{LW})/\alpha_{LW}$. Results are masked at the locations where the correlation between longwave heating rate and temperature is less than 0.7. The low correlation indicates a non-local and/or non-linear radiative damping, which is then not represented by the linear regression.

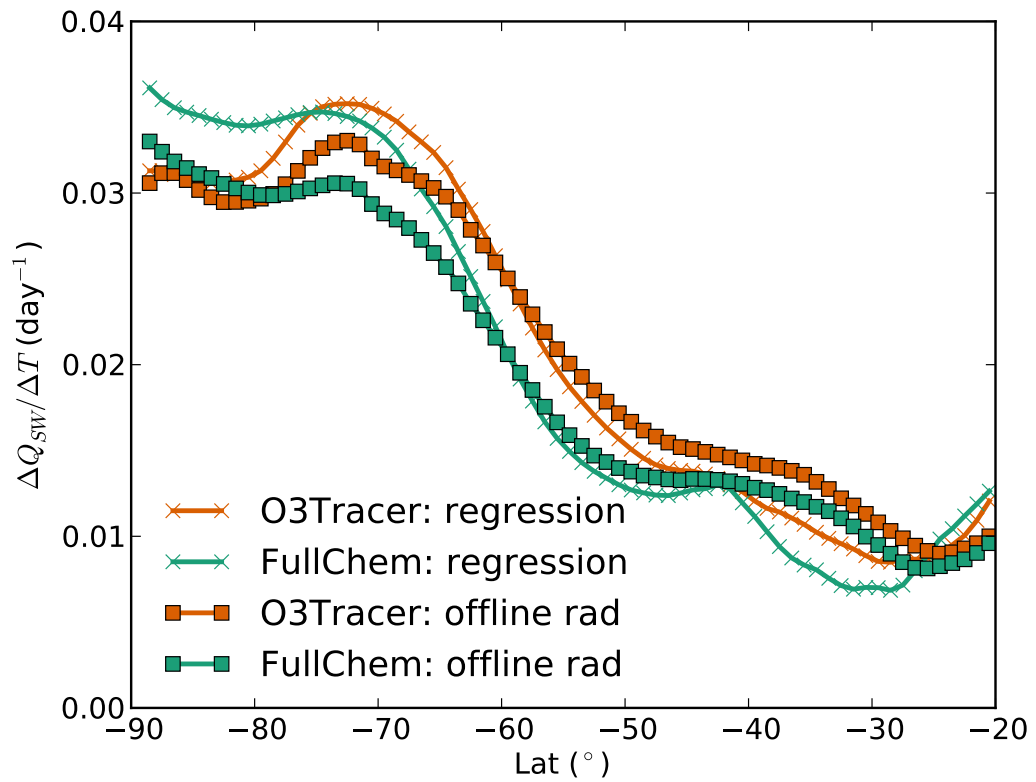


Figure 7. Shortwave heating rate associated with 1K warming at 50 hPa for November in *2010O3* simulations. Crosses indicate results from the regression between shortwave heating rate and temperature anomalies. Squares indicate results from the off-line radiative transfer calculation.

4 Summary and discussion

We simulate the climate response to stratospheric ozone depletion in GFDL AM4 with different ozone schemes: prescribing monthly zonal mean ozone concentration (CNTL), full stratospheric and tropospheric chemistry (FullChem) or prescribing monthly zonal mean chemical production rate and lifetime of ozone (O3Tracer). While similar amounts of ozone loss are produced by the three schemes, the resulting stratospheric cooling from prescribing ozone is significantly weaker than those from the other two schemes, with the largest difference occurring in November. We show that dynamics drive the difference in the stratospheric cooling. Compared to the two interactive ozone schemes, the CNTL simulation produces more wave dissipation in the lower stratosphere and less wave dissipation above, which leads to a stronger descending and dynamical warming in the polar lower stratosphere.

We identify two pathways that the dynamics respond to ozone depletion. The first one involves the strengthening of the polar vortex following the initial radiative cooling, which allows more wave dissipation in the stratosphere and enhances the dynamical heating at the polar lower stratosphere. This pathway has been well discussed in the literature (e.g., Li et al., 2008; McLandress & Shepherd, 2009; Lin et al., 2017) and is well represented in all three ozone schemes. The second pathway involves a modification of the radiative damping by ozone. With the existence of the ozone hole, large ozone anomalies co-vary with temperature anomalies. The shortwave heating from the ozone anomalies partly compensates the longwave cooling, leading to a weaker radiative damping. As a result, less wave dissipates at lower stratosphere, yielding to weaker dynamical heating over the polar region. This pathway builds on the coherence between ozone and circulation in their temporal and longitudinal variations, and hence is greatly suppressed when monthly zonal mean ozone is prescribed. On the other hand, in the two interactive ozone schemes, this second pathway does take effects and cancels with the first pathway, leading to no changes in the dynamical heating and stronger net cooling over the polar lower stratosphere.

We highlight the utility of the simplified ozone scheme O3Tracer. While its computational cost is as cheap as prescribing ozone and much cheaper than FullChem, it is capable of producing a ozone hole that is as strong as the one from FullChem and is capable of representing the interaction between ozone and circulation. It is also capable

360 of simulating the historical trend of stratospheric ozone when monthly time series of ozone
 361 production rate and lifetime are prescribed (not shown). The performance of O3Tracer
 362 degrades at the upper stratosphere and mesosphere where the coupling between the chem-
 363 ical reactions and the meteorology states becomes important. However, in many cases,
 364 the ozone changes in the lower stratosphere register a larger impact onto the climate sys-
 365 tem than those in the upper levels. Given the increased complexity of the climate mod-
 366 els that are not proportional to the increase of computational resources, the simplified
 367 ozone scheme may be a more practical and efficient choice for future climate model de-
 368 velopment.

369 **Appendix A Calculating coefficients needed for the O3Tracer scheme**

370 Rapid reactions occur between O and O₃, and the ozone concentration is not af-
 371 fected much by the cycling between the two. Instead, what controls the ozone concen-
 372 tration is the production rate of odd oxygen Ox, the sum of O and O₃. The Ox produc-
 373 tion rates can be directly diagnosed from the FullChem simulations, which includes the
 374 photolysis of oxygen as well as various chemical reactions considered in AM4. The life-
 375 time τ is calculated as

$$\tau = -X_{[O_3]}/(P - Q),$$

376 where $X_{[O_3]}$ is the ozone concentration, P is the Ox production rates, and Q is the net
 377 chemical tendency of ozone, all of which are outputted from the FullChem simulations.
 378 The monthly 3D fields of P and τ are then averaged zonally and averaged over the years.
 379 The resulting zonal mean monthly climatology is what the O3Tracer scheme uses.

380 Figure A1 shows P and τ used for the *2010O3* simulations in two representative
 381 months. As expected from the Chapman mechanism, ozone production rate generally
 382 follows the solar actinic flux, which increases with height and vanishes near the winter
 383 pole. The lifetime of ozone varies from years to minutes. Long lifetime is found in the
 384 upper troposphere and lower stratosphere, where ozone can be treated as a conservative
 385 tracer. Figure A1 also plots the difference in P and τ between the *2010O3* and *1960O3*
 386 simulations. Compared to the *1960O3* scenario, the *2010O3* case shows a modest increase
 387 of ozone production over the extratropical stratosphere and a reduction of ozone lifetime
 388 throughout the stratosphere.

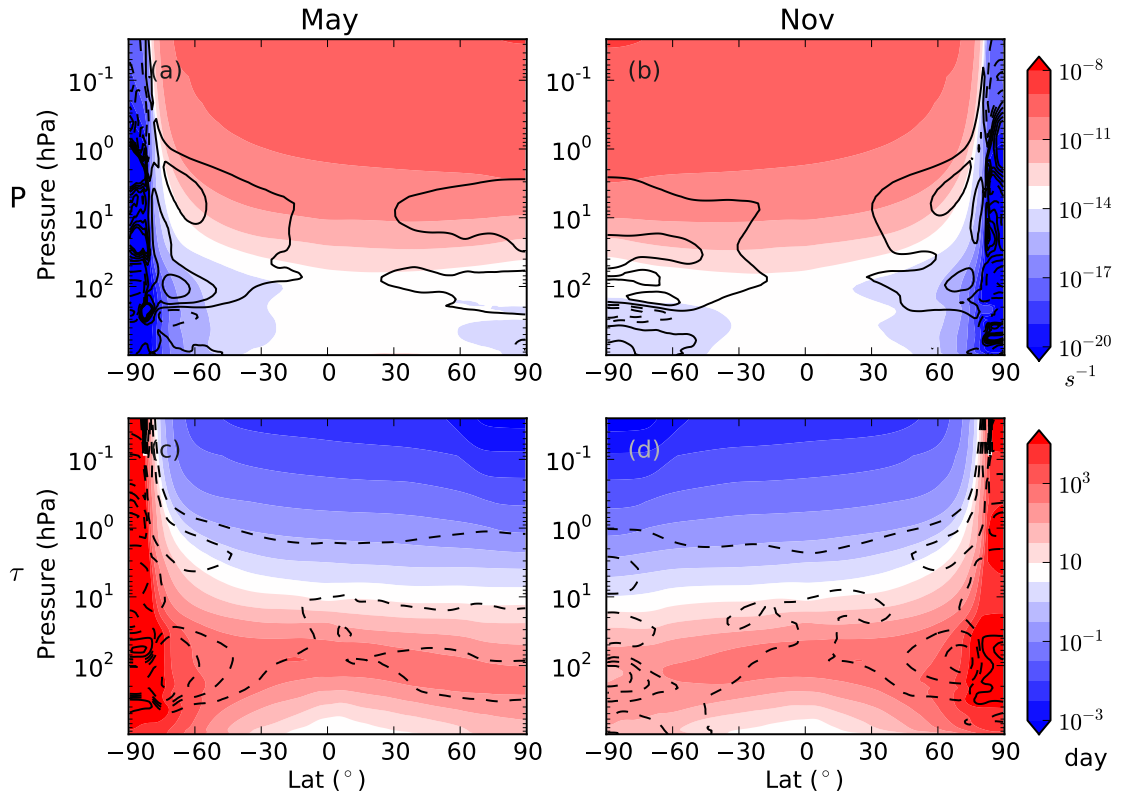


Figure A1. Coefficients used for 2010O3 O3Tracer simulations (color shading), and the relative difference between coefficients for 2010O3 and 1960O3 (contours). (a) Production rate in May. (b) Production rate in November. (c) Lifetime in May. (d) Lifetime in November. Contour intervals are -90% , -70% , ..., 70% , 90% . Negative contours are plotted in dashed lines.

389 **Acknowledgments**

390 We thank Larry W. Horowitz for his advice on constructing the O3Tracer scheme. This
 391 report was prepared by Pu Lin under award NA18OAR4320123 from the National Oceanic
 392 and Atmospheric Administration, U.S. Department of Commerce. The statements, find-
 393 ings, conclusions, and recommendations are those of the author(s) and do not necessar-
 394 ily reflect the views of the National Oceanic and Atmospheric Administration, or the U.S.
 395 Department of Commerce. The simulations used in the paper are permanently stored
 396 at the GFDL archive and are fully backed up. They are available upon request. The Fu-
 397 Liou radiative transfer code is provided by NASA Langley research center, available at:
 398 <https://cloudsgate2.larc.nasa.gov/cgi-bin/fuliou/lflcode/accesslfl.cgi>

399 **References**

- 400 Andrews, D. G., Holton, J. R., & Leovy, C. B. (1987). *Middle atmosphere dynamics*
 401 (Vol. 40). San Diego: Academic Press.
- 402 Austin, J., & Wilson, R. J. (2006). Ensemble simulations of the decline and recovery
 403 of stratospheric ozone. *J. Geophys. Res.*, *111*. doi: 10.1029/2005JD006907
- 404 Butchart, N. (2014). The Brewer-Dobson circulation. *Rev. Geophys.*, *52*, 157-184.
- 405 Cariolle, D., & Déqué, M. (1986). Souther Hemisphere medium-scale waves and total
 406 ozone disturbances in a spectral general circulation model. *J. Geophys. Res.*,
 407 *91*, 10825-10846.
- 408 Charney, J. G., & Drazin, P. G. (1961). Propagation of planetary scale disturbances
 409 from the lower into the upper atmosphere. *J. Geophys. Res.*, *66*, 83-109. doi:
 410 10.1029/JZ066i001p00083
- 411 Checa-Garcia, R., Hegglin, M. I., Kinnison, D., Plummer, D. A., & Shine, K. P.
 412 (2018). Historical tropospheric and stratospheric ozone radiative forc-
 413 ing using the cmip6 database. *Geophys. Res. Lett.*, *45*, 3264-3273. doi:
 414 10.1002/2017GL076770
- 415 Dunne, J. P., Horowitz, L. W., Adcroft, A. J., Ginoux, P., Held, I. M., John, J. G.,
 416 ... others (2020). The GFDL earth system model version 4.1 (GFDL-ESM
 417 4.1): Overall coupled model description and simulation characteristics. *J. Adv.*
 418 *Model. Earth Sy.*. doi: 10.1029/2019MS002015
- 419 Eyring, V., Arblaster, J. M., Cionni, I., Sedláček, J., Perlwitz, J., Young, P. J.,
 420 ... Watanabe, S. (2013). Long-term ozone changes and associated climate

- 421 impacts in CMIP5 simulations. *J. Geophys. Res.*, *118*, 5029-5060. doi:
422 10.1002/jgrd.50316
- 423 Fu, Q., & Liou, K.-N. (1992). On the correlated k-distribution method for radiative
424 transfer in nonhomogenous atmospheres. *J. Atmos. Sci.*, *49*, 2139-2156. doi:
425 10.1175/1520-0469(1992)049<2139:OTCDMF>2.0.CO;2
- 426 Geer, A. J., Lahoz, W. A., Jackson, D. R., Cariolle, D., & McCormack, J. P. (2007).
427 Evaluation of linear ozone photochemistry parameterizations in a stratosphere-
428 troposphere data assimilation system. *Atmos. Phys. Chem.*, *7*, 939-959.
- 429 Gerber, E. P., & Son, S.-W. (2014). Quantifying the summertime response of the
430 austral jet stream and Hadley cell to stratospheric ozone and greenhouse gases.
431 *J. Clim.*, *27*, 5538-5559. doi: 10.1175/JCLI-D-13-00539.1
- 432 Gillett, N. P., Scinocca, J. F., Plummer, D. A., & Reader, M. C. (2009). Sensitivity
433 of climate to dynamically consistent zonal asymmetries in ozone. *Geophys. Res.*
434 *Lett.*, *36*. doi: 10.1029/2009GL037246
- 435 Golaz, J.-C., Caldwell, P. M., Roedel, L. P. V., Petersen, M. R., Tang, Q., Wolfe,
436 J. D., ... others (2019). The DOE E3SM coupled model version 1: overview
437 and evaluation at standard resolution. *J. Adv. Model. Earth Sy.*, *11*, 2089-
438 2129. doi: 10.1029/2018MS001603
- 439 Haase, S., Fricke, J., Kruschke, T., Wahl, K., & Matthes, K. (2020). Sensitivity of
440 the southern hemisphere circumpolar jet response to Antarctic ozone depletion:
441 prescribed versus interactive chemistry. *Atmos. Phys. Chem.*, *20*, 14043-14061.
442 doi: 10.5194/acp-20-14043-2020
- 443 Haase, S., & Matthes, K. (2019). The importance of interactive chemistry for strato-
444 spheretroposphere coupling. *Atmos. Phys. Chem.*, *19*, 3417-3232. doi: 10.5194/
445 acp-19-3417-2019
- 446 Haynes, P. H., Marks, C. J., McIntyre, M. E., Shepherd, T. G., & Shine, K. P.
447 (1991). On the downward control of extratropical diabatic circulations by
448 eddy-induced mean zonal forces. *J. Atmos. Sci.*, *48*, 651-679.
- 449 Held, I. M., Guo, H., Adcroft, A., Dunne, J. P., Horowitz, L. W., Krasting, J., ...
450 Zadeh, N. (2019). Structure and performance of GFDL's CM4.0 climate
451 model. *J. Adv. Model. Earth Sy.*, *11*, 3691-3727. doi: 10.1029/2019MS001829
- 452 Hitchcock, P., Shepherd, T. G., & Yoden, S. (2010). On the approximation of lo-
453 cal and linear radiative damping in the middle atmosphere. *J. Atmos. Sci.*, *67*,

- 454 2070-2085. doi: 10.1175/2009JAS3286.1
- 455 Horowitz, L. W., Naik, V., Paulot, F., Ginoux, P. A., Dunne, J. P., Mao, J., ...
 456 Zhao, M. (2020). The GFDL global atmospheric chemistry-climate model
 457 AM4.1: model description and simulation characteristics. *J. Adv. Model. Earth*
 458 *Sy.* doi: 10.1029/2019MS002032
- 459 Keeble, J., Hassler, B., Banerjee, A., Checa-Garcia, R., Chiodo, G., Davis, S.,
 460 ... Wu, T. (2020). Evaluating stratospheric ozone and water vapor
 461 changes in CMIP6 models from 1850-2100. *Atmos. Phys. Chem. Disc.* doi:
 462 10.5194/acp-2019-1202
- 463 Li, F., Austin, J., & Wilson, J. (2008). The strength of the Brewer-Dobson circu-
 464 lation in a changing climate: coupled chemistry-climate model simulations. *J.*
 465 *Clim.*, *21*, 40-57. doi: 10.1175/2007JCLI1663.1
- 466 Li, F., Vikhliayev, Y. V., Newman, P. A., Pawson, S., Perlwitz, J., Waugh, D. W.,
 467 & Douglass, A. R. (2016). Impacts of interactive stratospheric chemistry on
 468 antarctic and southern ocean climate change in the Goddard Earth Observing
 469 System, version 5 (GEOS-5). *J. Clim.*, *29*, 3199-3218.
- 470 Lin, P., Paynter, D., Polvani, L., Correa, G. J. P., Ming, Y., & Ramaswamy, V.
 471 (2017). Dependence of model-simulated response to ozone depletion on strato-
 472 spheric polar vortex climatology. *Geophys. Res. Lett.*, *44*, 6391-6398. doi:
 473 10.1002/2017GL073862
- 474 McCormack, J. P., Eckermann, S. D., Coy, L., Allen, D. R., Kim, Y.-J., Hogan, T.,
 475 ... Trepte, C. R. (2004). NOGAPS-ALPHA model simulations of stratospheric
 476 ozone during the SOLVE2 campaign. *Atmos. Phys. Chem.*, *4*, 2401-2423. doi:
 477 10.5194/acp-4-2401-2004
- 478 McLandress, C., & Shepherd, T. G. (2009). Simulated anthropogenic changes in the
 479 Brewer-Dobson circulation, including its extension to high latitudes. *J. Clim.*,
 480 *22*, 1516-1540. doi: 10.1175/2008JCLI2679.1
- 481 McLinden, C. A., Olsen, S. C., Hannegan, B., Wild, O., & Prather, M. J. (2000).
 482 Stratospheric ozone in 3-d models: a simple chemistry and the cross-
 483 tropopause flux. *J. Geophys. Res.*, *105*, 14635-14665.
- 484 Michou, M., Nabat, P., Saint-Martin, D., Bock, J., Decharme, B., Mallet, M., ...
 485 Voldoire, A. (2019). Present-day and historical aerosol and ozone charac-
 486 teristics in CNRM CMIP6 simulations. *J. Adv. Model. Earth Sy.*, *12*. doi:

487 10.1029/2019MS001816

488 Monge-Sanz, B. M., Chipperfield, M. P., Cariolle, D., & Feng, W. (2011). Results
489 from a new linear o_3 scheme with embedded heterogeneous chemistry com-
490 pared with the parent full-chemistry 3-D CTM. *Atmos. Phys. Chem.*, *11*,
491 1227-1242. doi: 10.5194/acp-11-1227-2011

492 Neely, R. R., Marsh, D. R., Smith, K. L., Davis, S. M., & Polvani, L. M. (2014). Bi-
493 ases in Southern Hemisphere climate trends induced by coarsely specifying the
494 temporal resolution of stratospheric ozone. *Geophys. Res. Lett.*, *41*, 8602-8610.
495 doi: 10.1002/2014GL061627

496 Newman, P. A., & Randel, W. J. (1988). Coherent ozone-dynamical changes dur-
497 ing the southern hemisphere spring, 1979-1986. *J. Geophys. Res.*, *93*, 12585-
498 12606.

499 Polvani, L. M., Waugh, D. W., Correa, G. J. P., & Son, S. W. (2011). Strato-
500 spheric ozone depletion: the main driver of twentieth-century atmospheric
501 circulation changes in the Southern Hemisphere. *J. Clim.*, *24*, 795-812. doi:
502 10.1175/2010JCLI3772.1

503 Rae, C. D., Keeble, J., Hitchcock, P., & Pyle, J. A. (2019). Prescribing zonally
504 asymmetric ozone climatologies in climate models: Performance compared to a
505 chemistry-climate model. *J. Adv. Model. Earth Sy.*, *11*, 918-933.

506 Rieder, H. E., Chiodo, G., Fritzer, J., Wienerroither, C., & Polvani, L. M. (2019).
507 Is interactive ozone chemistry important to represent polar cap stratospheric
508 temperature variability in earth-system models? *Environ. Res. Lett.*, *14*,
509 044026. doi: 10.1088/1748-9326/ab07ff

510 Rose, F. G., & Charlock, T. P. (2002). New Fu-Liou code tested
511 with ARM Raman lidar and CERES in pre-CALIPSO exercise.
512 In *the 11th conference on atmospheric radiation*. Ogden, Utah.
513 (<https://ams.confex.com/ams/pdfpapers/42757.pdf>)

514 Schoeberl, M. R., & Hartmann, D. L. (1991). The dynamics of the stratospheric po-
515 lar vortex and its relation to springtime ozone depletions. *Science*, *251*, 46-52.
516 doi: 10.1126/science.251.4689.46

517 Solomon, S. (1999). Stratospheric ozone depletion: a review of concepts and history.
518 *Rev. Geophys.*, *37*, 275-316. doi: 10.1029/1999RG900008

519 Solomon, S., Portmann, R. W., Sasaki, T., Hofmann, D. J., & Thompson, D. W. J.

- 520 (2005). Four decades of ozonesonde measurements over Antarctica. *J. Geophys.*
521 *Res.*, *110*.
- 522 Son, S.-W., Gerber, E. P., Perlwitz, J., Polvani, L. M., Gillett, N. P., Seo, K.-H.,
523 ... others (2010). Impact of stratospheric ozone on Southern Hemisphere
524 circulation change: a multimodel assessment. *J. Geophys. Res.*, *115*. doi:
525 10.1029/2010JD014271
- 526 Son, S.-W., Polvani, L. M., Waugh, D. W., Akiyoshi, H., Garcia, R. R., Kinnison,
527 D., ... Shibata, K. (2008). The impact of stratospheric ozone recovery on the
528 Southern Hemisphere westerly jet. *Science*, *320*, 1486-1489.
- 529 Voldoire, A., Sanchez-Gomez, E., y Méliá dn B. Decharme, D. S., Cassou, C., Sénési,
530 S., Valcke, S., ... Chauvin, F. (2013). The CNRM-CM5.1 global climate
531 model: description and basic evaluation. *Clim. Dynam.*, *40*, 2091-2121. doi:
532 10.1007/s00382-011-1259-y
- 533 Waugh, D. W., Oman, L., Newman, P. A., Stolarski, R. S., Pawson, S., Nielsen,
534 J. E., & Perlwitz, J. (2009). Effect of zonal asymmetries in stratospheric ozone
535 on simulated Southern Hemisphere climate trends. *Geophys. Res. Lett.*, *36*.
536 doi: 10.1029/2009GL040419
- 537 Zhao, M., Golaz, J.-C., Held, I. M., Guo, H., Balaji, V., Benson, R., ... others
538 (2018a). The GFDL global atmosphere and land model AM4.0/LM4.0: 1.
539 simulation characteristics with prescribed ssts. *J. Adv. Model. Earth Sy.*, *10*,
540 691-734. doi: 10.1002/2017MS001208
- 541 Zhao, M., Golaz, J.-C., Held, I. M., Guo, H., Balaji, V., Benson, R., ... others
542 (2018b). The GFDL global atmosphere and land model AM4.0/LM4.0: 2.
543 model description, sensitivity studies, and tuning strategies. *J. Adv. Model.*
544 *Earth Sy.*, *10*, 735-769. doi: 10.1002/2017MS001209